

Supplementary Materials for

Wearable/disposable sweat-based glucose monitoring device with multistage transdermal drug delivery module

Hyunjae Lee, Changyeong Song, Yong Seok Hong, Min Sung Kim, Hye Rim Cho, Taegyung Kang, Kwangsoo Shin, Seung Hong Choi, Taeghwan Hyeon, Dae-Hyeong Kim

Published 8 March 2017, *Sci. Adv.* **3**, e1601314 (2017)
DOI: 10.1126/sciadv.1601314

This PDF file includes:

- Supplementary Text
- fig. S1. Optical camera images of the wearable diabetes patch.
- fig. S2. Device fabrication process.
- fig. S3. Schematic illustration of the operation sequence of the diabetes treatment system.
- fig. S4. Electrochemical analysis of the planar and porous gold electrode.
- fig. S5. Drug delivery from microneedles with integrated heaters.
- fig. S6. Effect of the sweat control layers and miniaturization of the glucose sensor.
- fig. S7. Characterization of the glucose sensor.
- fig. S8. Characterization of the pH sensor.
- fig. S9. Skin temperature and characterization of chlorpropamide-loaded PCNs.
- fig. S10. Characterization of hyaluronic acid, DOPA-conjugated hyaluronic acid.
- fig. S11. Characterization of the PCNs.
- fig. S12. Fabrication process of the microneedles.
- fig. S13. Characterization of the heater and temperature sensor and their cooperation.
- fig. S14. Portable electrochemical analyzer for the wearable diabetes patch.
- fig. S15. Reliability of the wearable diabetes patch under variable skin temperature and multiple reuses.
- fig. S16. Sweat uptake and calibration of the disposable strip-type sensors.
- fig. S17. Human sweat analysis.
- fig. S18. Feedback microneedle therapy.

Supplementary Text

Characterization of the humidity sensor

The humidity sensor is calibrated using the AC impedance method with an electrochemical analyzer (CHI660E, CHI Instruments, USA). Measurements are performed by the two-electrode method by using PEDOT-deposited interdigitated electrodes. The humidity sensor is calibrated by measuring its impedance changes and adding an artificial sweat solution. The impedance–time measurements are used for real-time humidity monitoring.

Characterization of the glucose sensor

i) Calibration process: The glucose sensor is characterized by the galvanostatic method with an electrochemical analyzer (CHI660E, CHI Instruments, USA). The three-electrode method is used for the measurement. The three electrodes include an enzyme layer/PB/porous gold-deposited working electrode, a Pt counter electrode, and an Ag/AgCl reference electrode. The galvanostatic measurement is conducted at an initial potential of -0.2 V for 20 s for each measurement using the artificial sweat solution with glucose concentrations from 0 to 1 mM (Product #G5767, Sigma-Aldrich, USA) in 1X PBS (Dulbecco's phosphate-buffered saline, WELGENE Inc., Republic of Korea).

ii) Other characterizations: Other characterizations are performed by the same procedure of the calibration process. The stretching test is conducted under 0–20 % applied strains. The temperature dependency of the glucose sensor is tested with the artificial sweat solution between 20 and 45 °C. The selectivity of the glucose sensor is tested with the solution of PBS, 0.1 mM glucose, 10 μ M ascorbic acid (Product #A7506, Sigma-Aldrich, USA), 59 μ M uric acid (Product #U2625, Sigma-Aldrich, USA), 4 mM lactic acid (Product #69775, Sigma-Aldrich, USA), 132 μ M acetaminophen (Product #A7085, Sigma-Aldrich, USA), 555 μ M acetylsalicylic acid (Product #A5376, Sigma-Aldrich, USA), and 774 μ M metformin (Product #D150959, Sigma-Aldrich, USA). For long-term stability test over several days, the glucose sensor is tested under room temperature and

stored at 4 °C when it is not used. The pH dependency of the glucose sensor is estimated with the artificial sweat solution at pH values of 4 to 7.

Characterization of the pH sensor

The pH sensor is characterized through the open circuit potential (OCP) measurement with an electrochemical analyzer (CHI660E, CHI Instruments, USA). The two-electrode method is used for the measurement. The two electrodes are a PANi-deposited working electrode and an Ag/AgCl-deposited counter electrode. The pH sensor is calibrated using standard buffered pH solutions (pH of buffered solutions from 4 to 7, Alfa Aesar, USA). The stretching test is conducted under 0–20 % applied strains. The temperature dependency of the pH sensor is tested between 20 °C and 45 °C.

Characterization of the heater and temperature sensor

The heater temperature is controlled by the power supply module (U8031A, Agilent, USA). The temperature is monitored with an IR camera (FLIR E8, FLIR, USA). The temperature sensors in the wearable sweat glucose sensors and the transdermal drug delivery device are calibrated using a semiconductor device analyzer (B1500A, Agilent, USA).

Glucose level measurement process using glucose and pH sensors

The glucose and pH sensors are calibrated before their first use. The galvanostatic measurement is performed by the glucose sensor, which gives a current (i) versus time (t) curve under the constant potential (initial potential: -0.2 V vs Ag/AgCl). The measured current is converted into the glucose concentration based on the calibration curve (Fig. 2F bottom). For pH monitoring, the measured open circuit potential is converted into the pH value by using the calibration curve (fig. S8A). The measured pH value is then used to adjust the glucose concentration (Fig. 2I and fig. S7F).

Synthesis procedure and characterization of phase change nanoparticles

0.5 g of PCM for PCN1 (palm oil; Product #70905, Sigma-Aldrich, USA) or PCN2 (tridecanoic acid; Product #T0412, Tokyo Chemical Industry, Japan), 0.03 g of F127 (Product #P2443, Sigma-Aldrich, USA), 0.02 g of DOPA-conjugated hyaluronic acid, and metformin (Product #D150959, Sigma-Aldrich, USA) or chlorpropamide (Product #C129531, Aladdin, USA) are dissolved in water. In case of the releasing test, rhodamine B dye is added to the solution to visualize and analyze the loading and releasing of drugs into and from PCNs in the microneedle matrix. The solution is sonicated for 30 min with a probe-type ultra-sonicator. The nuclear magnetic resonance (NMR) data of HA and DOPA-conjugated HA are obtained using Avance-500 (Bruker) at National Center for Inter University Research Facilities (NCIRF). PCN1 and PCN2 are observed by cryo-TEM and TEM. The hydro-diameter and zeta potential of PCNs are measured at skin temperature (30 °C) and drug delivery temperatures (40 °C, 45 °C) by Zetasizer Nano S90. Dye release from the PCNs is measured with a photoluminescence spectrometer (λ_{em} : 570 nm) while changing the temperature from 30 °C (skin temperature) to 45 °C (drug-release temperature).

In vitro characterization of microneedles

Dissolution of PCM-coated and PCM-uncoated microneedles is tested in the PBS. The rigidity of the microneedles is measured with the universal testing machine (maximum weight: 10 N, scan rate: 0.1 mm s⁻¹). To observe the penetration of the microneedles, a tissue-like 4 % agarose gel is used, and the penetration is examined by a confocal laser fluorescence microscope. Thermal actuation by the heater and the corresponding dye release into the agarose gel are imaged by an IR camera (FLIR E8, FLIR, USA) and a confocal laser fluorescence microscope. The dye-release profile of the PCM-coated microneedles is measured during the temperature change from 30 °C (skin temperature) to 45 °C (drug-release temperature). The multi-stage dye release with the three-channel thermal actuation is measured by the photoluminescence spectrometer (λ_{em} : 570 nm). In the case of the hot weather, external temperature can reach beyond the transition temperature. In this condition, other phase change materials (PCMs) can be used for a higher melting temperature.

Human sweat analysis

Human sweat study is performed in compliance with the protocol approved by the institutional review board at the Seoul National University (IRB No. 1605/003-002). Five healthy subjects, aged 20–60 years, participated in the study. All subjects are informed of the risks and benefits, and they provided informed consent. For obtaining the correlation factor between glucose levels in sweat and blood, the blood glucose level is tested using a commercial glucose meter (Accu-Check Performa, Roche, Switzerland) 1 h before and after a meal. After testing the blood glucose level, a sweat monitoring patch is attached on the skin to monitor sweat hydration, glucose/pH levels, and temperature while the subject uses a cycle ergometer. The sweat monitoring patch is integrated with a sweat-uptake layer (wood pulp and Rayon; SWISSPURE half sponge sheet, Able C&C, Republic of Korea) and a water-proof layer (Tegaderm 1624W, 3M, USA) for efficient sweat collection. For the electrochemical measurement, the sweat monitoring patch is connected to a portable electrochemical analyzer (PalmSens3, Palm instrument B.V., Netherlands) via an anisotropic conductive film (HST-9805-210, Elform, USA). To examine the accuracy of the sweat glucose monitoring result, the glucose level measured from the patch is compared with a glucose level measured by a commercial glucose assay (Glucose assay kit, Cayman chemical, USA). The sweat analysis patch should be newly attached on the skin for each sweat glucose measurement after removing previously collected sweat. Typically the time taken for cleaning and reattachment of the patch is ~10 min. We therefore developed a disposable strip-type sensor for easy and fast replacement of the sensing system.

In vivo characterization of microneedles

In vivo experiment of the microneedles is conducted using 8-to-12-week-old db/db mice. All mice were fasted overnight before the experiment. The drug-loaded microneedles are attached to the shaved abdomen skin of the db/db mouse with a gentle pressure. The transcutaneous drug delivery is started with the thermal actuation by the embedded heater. The change in the blood glucose levels is measured using a commercial glucose meter (Accu-chek performa, Roche, Switzerland).

Ethical approval for the animal experiment

All procedures are approved by the Institutional Animal Care and Use Committee (IACUC) of the Biomedical Research Institute of Seoul National University Hospital. All experiments are performed according to IACUC guidelines.

Supplementary Figures

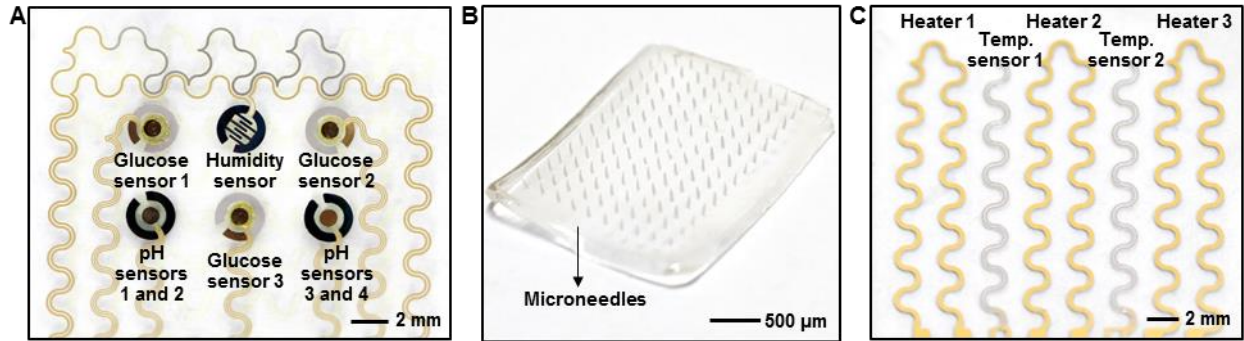


fig. S1. Optical camera images of the wearable diabetes patch. (A) Optical camera image of wearable sweat analysis sensors. (B) Optical camera image of thermo-responsive and bioresorbable microneedles. (C) Optical camera image of a transdermal drug delivery device before integrating the microneedles.

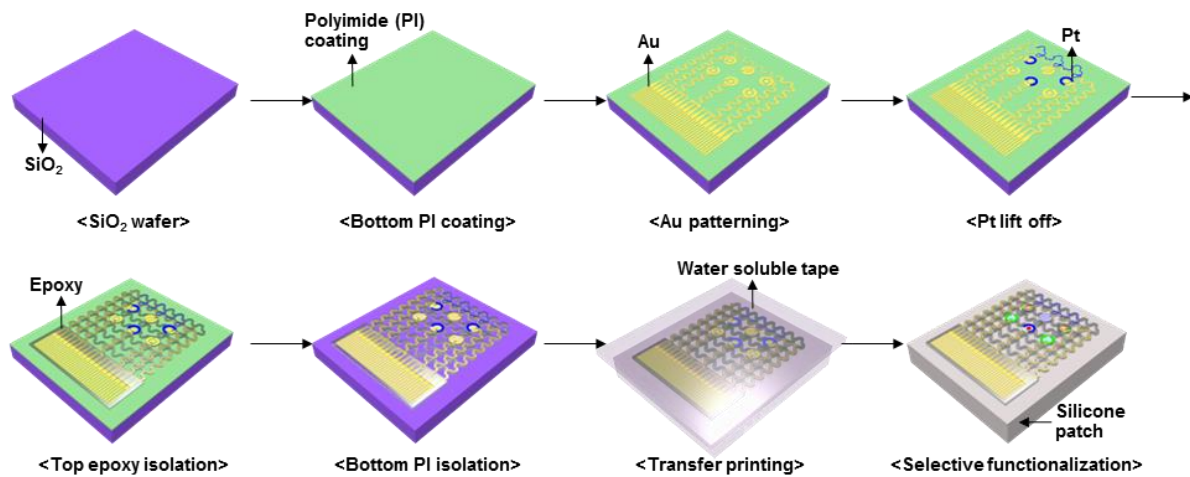


fig. S2. Device fabrication process. Schematic illustration of the fabrication process of the sweat analysis sensors.

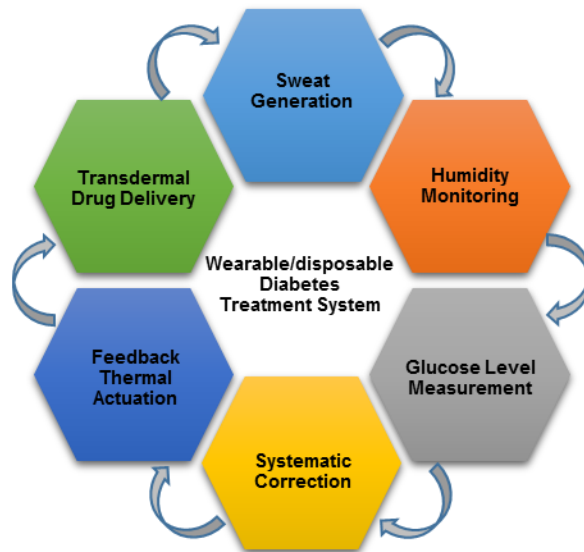


fig. S3. Schematic illustration of the operation sequence of the diabetes treatment system. After wearing the diabetes patch, generated sweat from the skin will be absorbed by the sweat-uptake layer. First, the humidity sensor monitors the amount of sweat. When the accumulated sweat amount is sufficient for the measurement, glucose is measured with real-time correction by using pH and temperature measurements. When hyperglycemia occurs, the drug-loaded microneedles are activated by thermal actuation, and the transdermal drug delivery proceeds.

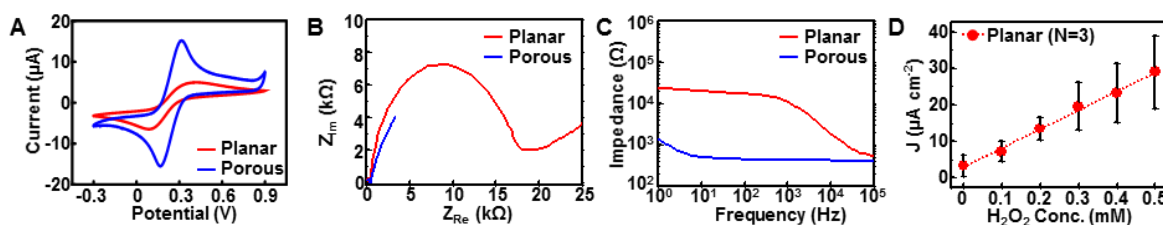


fig. S4. Electrochemical analysis of the planar and porous gold electrode. (A) CV plots of the planar and porous gold electrode in PBS with $\text{Fe}(\text{CN})_6^{3-/4-}$ (scan rate: 0.1 V s^{-1} with the commercial Ag/AgCl electrode). (B) Nyquist plots of the planar and porous gold electrode in PBS with $\text{Fe}(\text{CN})_6^{3-/4-}$ at the equilibrium potential used in fig. S4A. (C) Bode plots of the planar and porous gold electrode in PBS with $\text{Fe}(\text{CN})_6^{3-/4-}$ at the equilibrium potential used in fig. S4A. (D) The H_2O_2 sensitivity in the planar gold electrode deposited with Prussian blue at different H_2O_2 concentrations.

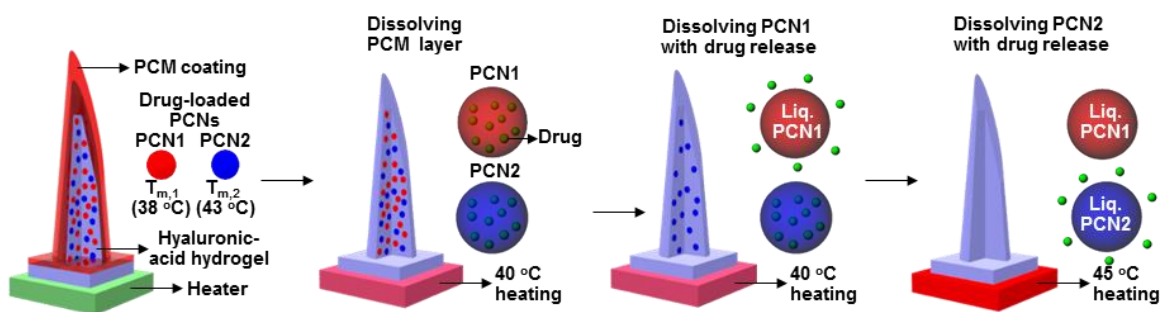


fig. S5. Drug delivery from microneedles with integrated heaters. Drug release from microneedles can be controlled by stepwise thermal actuation of integrated heater.

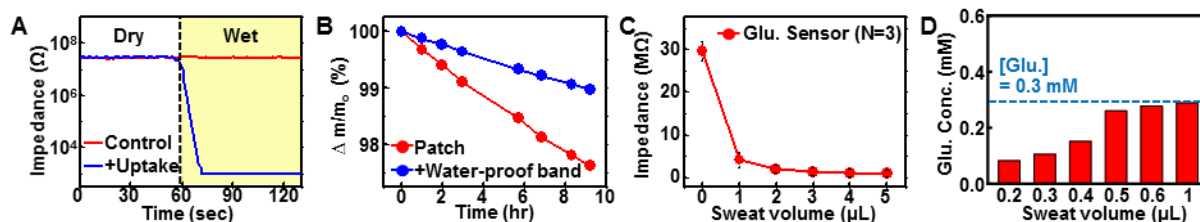


fig. S6. Effect of the sweat control layers and miniaturization of the glucose sensor. (A) Impedance change of the humidity sensor with (blue) and without (red) a sweat-uptake layer during addition of artificial sweat. (B) Relative mass change of water by evaporation with (blue) and without (red) the water-proof band. (C) Impedance change of the glucose sensor at different volumes of the artificial sweat solution. (D) Glucose concentration measurement at different sweat volumes (0.3 mM glucose in artificial sweat).

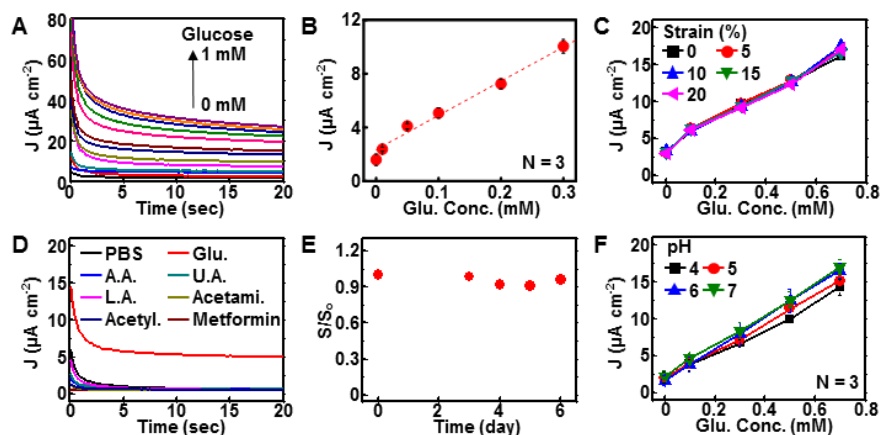


fig. S7. Characterization of the glucose sensor. (A) Chronoamperometric response of the glucose sensor to increasing glucose concentrations from 0 to 1 mM. (B) Calibration curve of the glucose sensor at sweat glucose levels (glucose concentration: from 0 to 0.3 mM). (C) Calibration curves of the glucose sensor at different applied strains. (D) Chronoamperometric response of the glucose sensor to PBS, 0.1 mM Glucose (Glu.), 10 μ M ascorbic acid (A.A.), 59 μ M uric acid (U.A.), 4 mM lactic acid (L.A.), 132 μ M acetaminophen (Acetami.), 555 μ M acetylsalicylic acid (Acetyl.), and 774 μ M (metformin). Each concentration is selected as the value commonly found in the human sweat. (E) Long-term stability of the glucose sensor. The relative sensitivity (S/S_0) is defined as measured sensitivity divided by initial sensitivity. (F) Calibration curves of the glucose sensor at different pH levels.

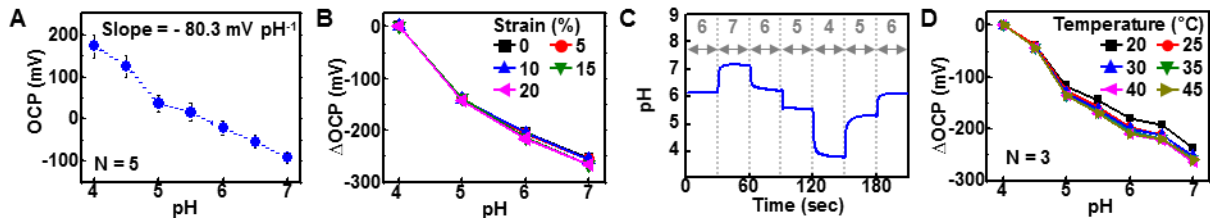


fig. S8. Characterization of the pH sensor. (A) OCP changes of the pH sensor. (B) pH-dependent OCP changes of the pH sensor at different applied strains. (C) Characterization of the pH sensor in standard buffered solutions whose pH changes are 6→7→6→5→4→5→6. (D) OCP changes of the pH sensor at different temperatures.

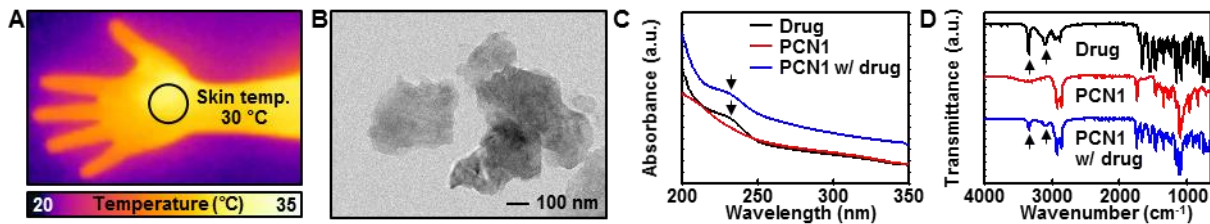


fig. S9. Skin temperature and characterization of chlorpropamide-loaded PCNs. (A) IR camera image of human skin. (B) TEM image of chlorpropamide-loaded PCNs. (C) Ultraviolet–visible spectroscopy data of chlorpropamide (drug, black), PCN1 (palm oil, red), and drug-loaded PCN1 (blue). (D) Fourier transform infrared spectroscopy of chlorpropamide (drug, black), PCN1 (palm oil, red), and drug-loaded PCN1 (blue).

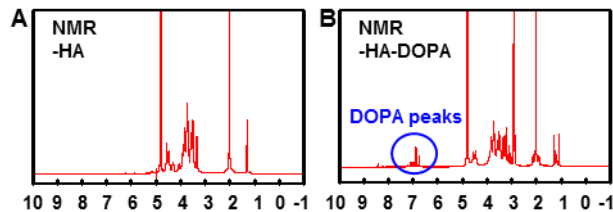


fig. S10. Characterization of hyaluronic acid, DOPA-conjugated hyaluronic acid. (A) Nuclear magnetic resonance analysis data of hyaluronic acid. (B) Nuclear magnetic resonance analysis data of DOPA-conjugated hyaluronic acid.

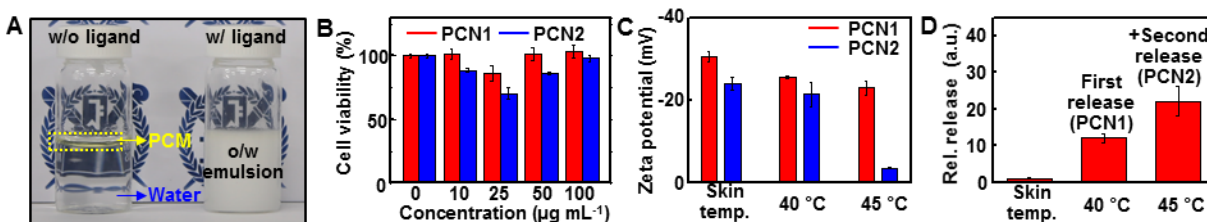


fig. S11. Characterization of the PCNs. (A) Optical image of dispersed PCNs without (left) and with (right) ligands. (B) Cell viability test at different concentrations of PCNs (4 h exposure). (C) Zeta potential measurement of PCNs at 30 (skin temperature), 40, and 45 °C. (D) Step-wise drug delivery of PCNs at 30 (skin temperature), 40, and 45 °C.

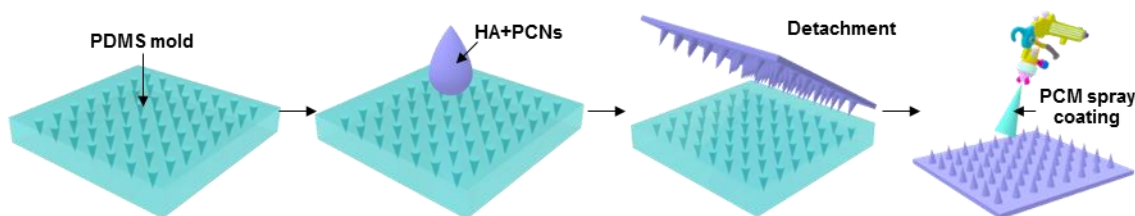


fig. S12. Fabrication process of the microneedles. Schematic illustration of the fabrication process of the microneedles. Microneedles are made of two types of drug-loaded PCNs and a hyaluronic acid matrix. They are coated with a biocompatible PCM after detaching from the mold.

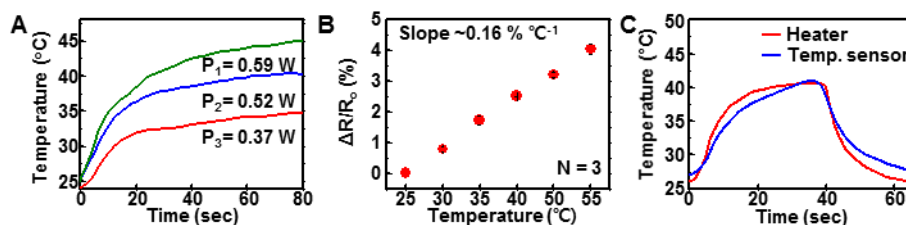


fig. S13. Characterization of the heater and temperature sensor and their cooperation. (A) Output temperature profiles of the heater at different powers (P₁-P₃). (B) Characterization of the temperature sensor. (C) In situ temperature monitoring of the heater by using a commercial IR camera and the integrated temperature sensor.

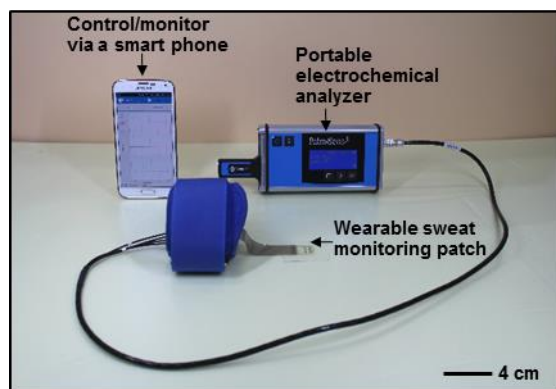


fig. S14. Portable electrochemical analyzer for the wearable diabetes patch. The wearable sweat monitoring patch is connected to a portable electrochemical analyzer that supplies power and controls the patch. The portable electrochemical analyzer can communicate with commercial mobile devices wirelessly via Bluetooth.

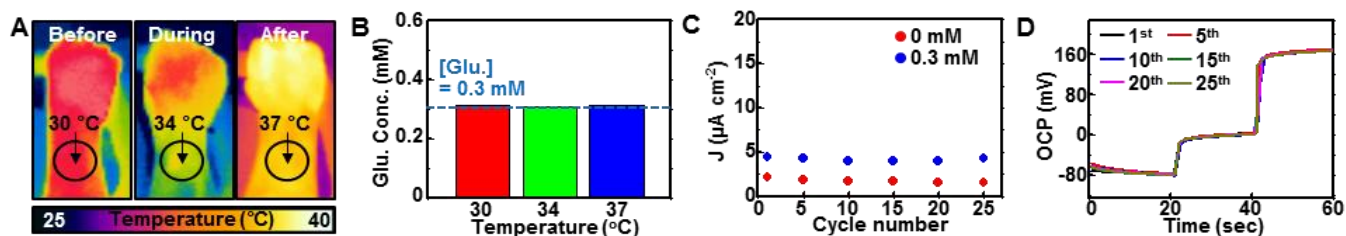


fig. S15. Reliability of the wearable diabetes patch under variable skin temperature and multiple reuses.

(A) IR camera image of the human skin before, during, and after using a cycle ergometer. (B) Stable glucose sensing of the artificial sweat (0.3 mM glucose) at the skin temperature of 30, 34, and 37 °C. (C) Stable glucose sensing of the artificial sweat (0.1 mM glucose) after multiple reuses. (D) Stable pH sensing by using standard buffer solutions (pH 6→5→4) after multiple reuses.

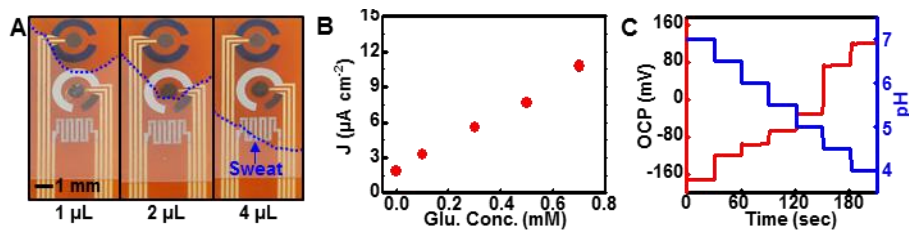


fig. S16. Sweat uptake and calibration of the disposable strip-type sensors. (A) Optical camera images of the sweat uptake through the fluidic channel at the tip of the strip for sweat saturation. (B) Calibration curves of the strip-type glucose sensor by using artificial sweat solutions. (C) Calibration curves of the strip-type pH sensor.

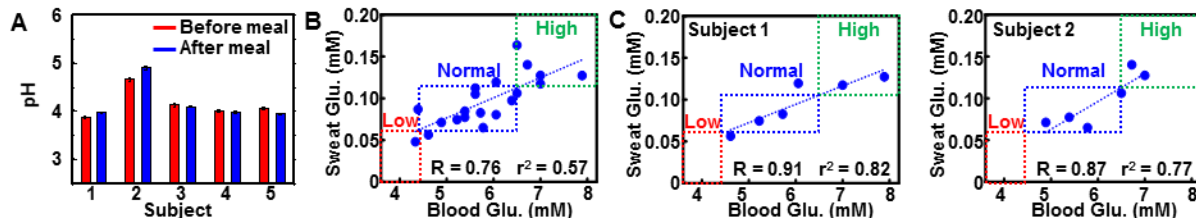


fig. S17. Human sweat analysis. (A) Measurement of pH levels ($N = 4$) in sweat from five subjects before and after a meal. (B) Statistical analysis of the correlation between the sweat glucose concentrations and the blood glucose concentrations ($N = 20$, $R = 0.76$ from Pearson's correlation test, $r^2 = 0.57$ from linear regression analysis). (C) Statistical analysis of the correlation between the sweat glucose concentrations and the blood glucose concentrations for two subjects ($N = 6$ for each subject).

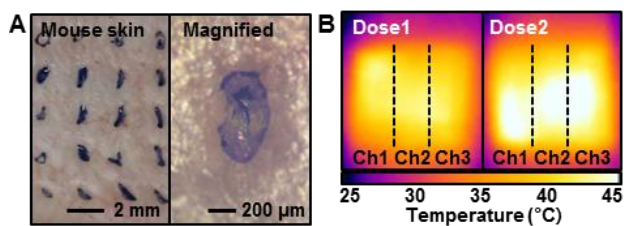


fig. S18. Feedback microneedle therapy. (A) Optical camera images of the mouse skin with the trypan blue staining (left) and its magnified view (right). (B) IR camera images of the thermal actuation for the transdermal drug delivery (dose1: $40\text{ }^{\circ}\text{C}$, dose2: $45\text{ }^{\circ}\text{C}$).